Opposing chemokine gradients control human thymocyte migration in situ

Joanna Halkias,[1,2] Heather J. Melichar,[1] Kayleigh T. Taylor,[1] Jenny O. Ross,[1] Bonnie Yen,[1] Samantha B. Cooper,[3] Astar Winoto,[1] and Ellen A. Robey[1]

[1]Division of Immunology and Pathogenesis, Department of Molecular and Cell Biology, UC Berkeley, Berkeley, California, USA.
[2]Division of Neonatology, Children's Hospital and Research Center Oakland, Oakland, California, USA.
[3]Department of Cellular and Molecular Pharmacology, UCSF, San Francisco, California, USA.

The ordered migration of thymocytes from the cortex to the medulla is critical for the appropriate selection of the mature T cell repertoire. Most studies of thymocyte migration rely on mouse models, but we know relatively little about how human thymocytes find their appropriate anatomical niches within the thymus. Moreover, the signals that retain $CD4^+CD8^+$ double-positive (DP) thymocytes in the cortex and prevent them from entering the medulla prior to positive selection have not been identified in mice or humans. Here, we examined the intrathymic migration of human thymocytes in both mouse and human thymic stroma and found that human thymocyte subsets localized appropriately to the cortex on mouse thymic stroma and that MHC-dependent interactions between human thymocytes and mouse stroma could maintain the activation and motility of DP cells. We also showed that CXCR4 was required to retain human DP thymocytes in the cortex, whereas CCR7 promoted migration of mature human thymocytes to the medulla. Thus, 2 opposing chemokine gradients control the migration of thymocytes from the cortex to the medulla. These findings point to significant interspecies conservation in thymocyte-stroma interactions and provide the first evidence that chemokines not only attract mature thymocytes to the medulla, but also play an active role in retaining DP thymocytes in the cortex prior to positive selection.

Introduction

The thymus consists of distinct anatomical compartments dedicated to the support of different phases of T cell development. Accordingly, thymocyte maturation is tightly coupled to intrathymic migration (1, 2). The thymic cortex harbors immature $CD4^+CD8^+$ double-positive (DP) thymocytes as well as specialized epithelial cells that provide positive selection signals. The thymic medulla, on the other hand, contains more mature $CD4^+CD8^-$ or $CD4^-CD8^+$ single-positive (SP) thymocytes, as well as a unique epithelial cell population that expresses a range of tissue-restricted antigens and a higher concentration of DCs to present self-antigens for negative selection. Mutations that disrupt normal thymic migration patterns can lead to autoimmunity, highlighting the importance of appropriate migration for selection of the T cell repertoire (3–5).

The thymic medulla expresses a number of chemokines, and there is ample evidence that the CCR7-CCL19/21 axis promotes migration of mouse thymocytes from the cortex to the medulla at the DP-to-SP developmental transition (6–8). In contrast, only 2 chemokines, CXCL12 (also known as SDF-1) and CCL25 (also known as TECK), are known to be expressed at higher levels in the cortex relative to the medulla (2, 9). Mouse and human DP thymocytes migrate toward CXCL12 and CCL25 in vitro, but it is unclear whether they respond similarly in vivo (10, 11). Mice lacking expression of the CXCL12 receptor, CXCR4, on thymocytes showed defective $CD4^-CD8^-$ double-negative (DN) thymocyte migration from the subcapsular region to the cortex as well as defects in DN-to-DP transition. However, no defects in the cortical segregation of DP thymocytes or the DP-to-SP developmental transition were observed (12–14). In addition, mouse DP thymocytes express proteins that dampen their responses to cortical chemokines (15, 16). Indeed, it has been suggested that retention of DP thymocytes in the cortex prior to positive selection is independent of chemokine signaling and may instead occur via a passive mechanism, such as the inability of DP thymocytes to migrate on medullary extracellular matrix (2, 8).

In addition to the dearth of knowledge about signals that retain DP thymocytes in the cortex, it is noteworthy that virtually all of our information about intrathymic migration comes from mouse studies. Mice and humans differ in basic thymus anatomy, such as the presence of well-developed Hassall's corpuscles in the thymic medulla of humans, but not mice. Moreover, thymocyte ontogeny and cell surface phenotype of developmental intermediates differ significantly between mice and humans (17–19). Thus, studying human thymic samples will undoubtedly reveal unique information distinct from that obtained from studies of mouse models.

Humanized immune system (HIS) mice, in which human thymocytes develop on mouse thymic stroma, provide in vivo models for examining human immune responses (20), but molecular understanding of interspecies crosstalk in these systems is lacking. While there are indications that some human thymocytes can be selected on mouse MHC molecules, it is currently unclear to what extent human thymocytes engage mouse MHC (21–23). In addition, T cell development in HIS mice may be limited by suboptimal interactions between other mouse-human receptor-ligand pairs, including chemokines, cytokines, and their receptors (24). Thus, a greater knowledge of the interspecies interactions between human thymocytes and mouse thymic stroma is needed to optimize human T cell development in these models.

Authorship note: Joanna Halkias and Heather J. Melichar contributed equally to this work.

Conflict of interest: The authors have declared that no conflict of interest exists.

Citation for this article: *J Clin Invest.* 2013;123(5):2131–2142. doi:10.1172/JCI67175.

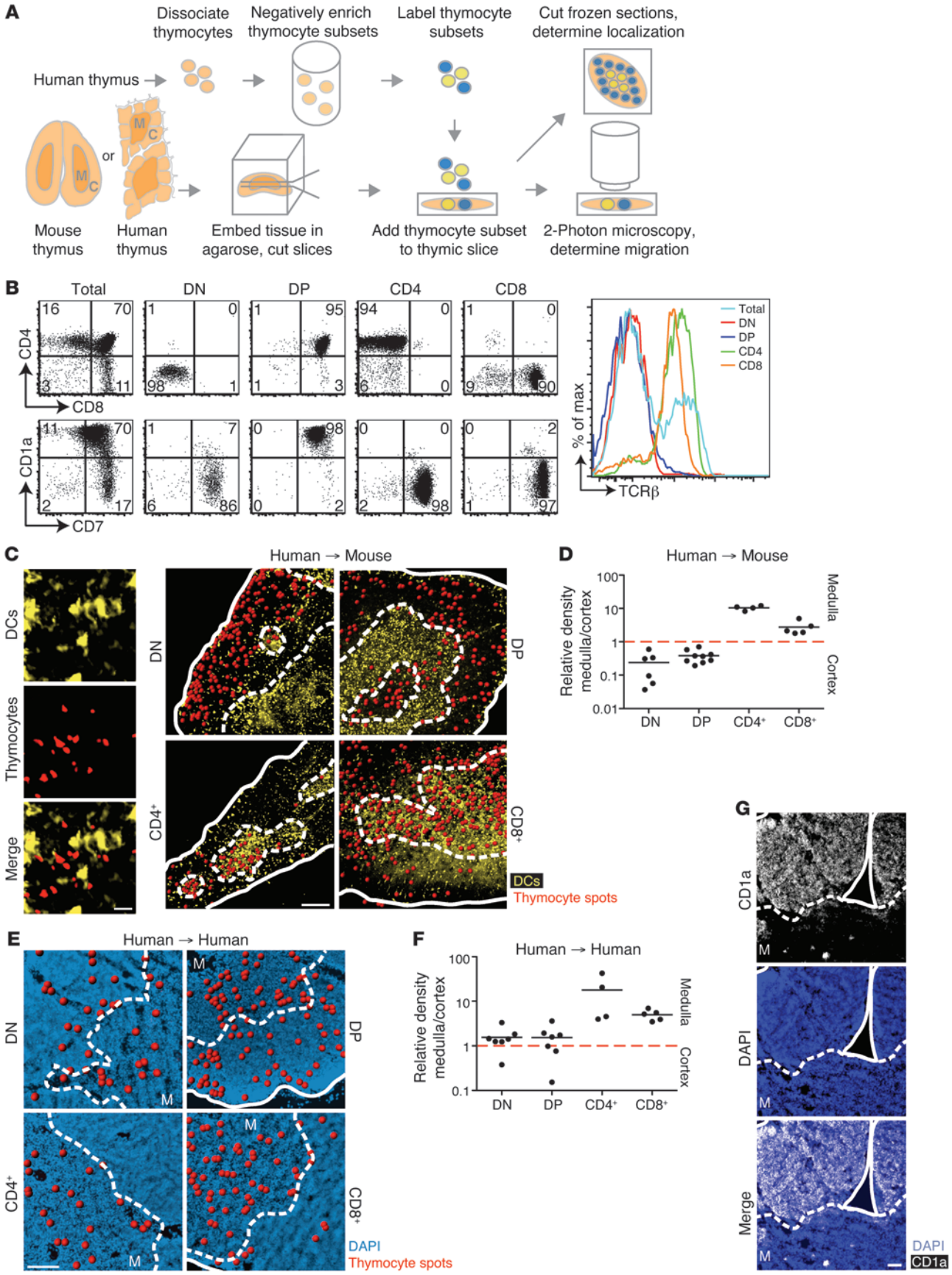
A
Dissociate thymocytes
Negatively enrich thymocyte subsets
Label thymocyte subsets
Cut frozen sections, determine localization
Human thymus
or
Mouse thymus
Human thymus
Embed tissue in agarose, cut slices
Add thymocyte subset to thymic slice
2-Photon microscopy, determine migration
B
Total
DN
DP
CD4
CD8
CD4
CD8
CD1a
CD7
% of max
TCRβ
C
Human → Mouse
DCs
Thymocytes
Merge
DN
DP
CD4+
CD8+
DCs
Thymocyte spots
D
Human → Mouse
Relative density medulla/cortex
Medulla
Cortex
DN
DP
CD4+
CD8+
E
Human → Human
DAPI
Thymocyte spots
F
Human → Human
G
CD1a
DAPI
Merge
DAPI
CD1a

Figure 1
Human thymocyte subsets localize appropriately on mouse thymic slices. (**A**) Experimental setup. Human thymic slices were prepared from a tissue fragment containing both cortex (C) and medulla (M). (**B**) Flow cytometric analysis of purified human thymocyte subsets. (**C**) Representative fixed cryosections for localization of human thymocytes overlaid on CD11c-YFP transgenic mouse thymic slices. Red spots denote thymocyte signals; solid outlines denote tissue edge; dashed outlines delineate corticomedullary junction. Individual views of CD11c-YFP signal, SNARF-labeled thymocytes, and merged image are shown at left. (**D**) Relative density of each human thymic subset on mouse thymic slices. Each dot represents quantification of 1 tissue section. n = 635 cells (DN); 3,607 cells (DP); 856 cells ($CD4^+$); 1,779 cells ($CD8^+$). (**E**) Representative fixed cryosections of human thymocyte subsets overlaid on human thymic slices. DAPI staining (blue) was used to distinguish cortex from medulla. (**F**) Relative density of human thymic subsets on human thymic slices. n = 199 cells (DN); 1,403 cells (DP); 558 cells ($CD4^+$); 420 cells ($CD8^+$). (**G**) Immunofluorescent stain of fixed cryosections of human thymus with CD1a and DAPI. Scale bars: 20 μm (**C**, left); 200 μm (**C**, right); 100 μm (**E**); 50 μm (**G**).

Here, we used a thymic slice model in conjunction with 2-photon time-lapse microscopy to examine human thymocyte migration in 3-dimensional living tissue (8, 25). This allowed us to characterize the motility and localization of human thymocytes on both mouse and human thymic stroma and to probe the mechanisms that direct these behaviors. We found that human thymocytes showed appropriate intrathymic localization and developmentally regulated changes in motility on mouse stroma. Furthermore, we found that interspecies recognition of mouse MHC could maintain the activation and motility of human DP thymocytes on mouse stroma. We also provide evidence that 2 distinct chemokine receptors contributed to the correct localization of mature versus immature human thymocytes: CCR7 signals promoted SP localization to the medulla, and CXCR4 signals promoted DP thymocyte localization to the cortex. These data suggest that positive selection and the transition from the DP to the SP stage of thymic development involves both the loss of attraction to cortical chemokines and the acquisition of responsiveness to medullary chemokines; furthermore, our results revealed extensive interspecies crosstalk between human thymocytes and mouse thymic stroma.

Results

Human thymocyte migration in mouse and human thymic environments. In order to examine human thymocyte migration in situ, we adapted a protocol initially developed for mouse tissues (8, 25): isolated thymocyte populations were applied to a vibratome-cut thymic slice, and their location and migration patterns were examined after short-term culture (Figure 1A). Because human T cells can develop in a murine thymic environment (20, 26), we focused our attention on the behavior of human thymocytes on murine thymic slices. This interspecies slice model allowed us to take advantage of genetic manipulations available in mice and provided information about interspecies conservation in thymocyte-stroma interactions. We isolated human thymocyte populations from 18- to 20-week fetal thymic tissue using negative enrichment procedures to eliminate any abnormal behavior that might result from artificially blocking or activating surface molecules. We consistently isolated DN and $CD69^-TCR\beta^{lo}$ DP thymocytes as well as mature $CD1a^-$ SP thymocyte subsets (either $CD4^+$ or $CD8^+$) with greater than 85% purity (Figure 1B). Subset purity was verified, and costaining with CD7 allowed confirmation of T lineage commitment, while CD1a and TCRβ allowed for a more detailed characterization of the maturational state of the thymic subsets. Human purified thymocytes were then labeled with fluorescent dyes and allowed to migrate into mouse or human thymic slices for 2–4 hours. In most experiments with mouse thymic slices, we used mice expressing a DC-specific fluorescent reporter, CD11c-YFP, to aid in distinguishing cortex from medulla (27, 28). Samples were either imaged by 2-photon microscopy to examine thymocyte migration patterns or fixed, frozen, and further sectioned for microscopy to examine thymocyte localization patterns (Figure 1A).

We first asked whether human thymocytes would migrate into murine thymic tissue and correctly localize to their expected microenvironment. Microscopy of fixed, frozen thymic sections showed that immature DN and DP human thymocytes were largely confined to the cortex, whereas mature $CD4^+$ and $CD8^+$ SP populations were preferentially located in the medulla (Figure 1, C and D). Our findings — consistent with previous studies in mice (8) — indicate that the thymocyte-stromal cell signals that direct thymocyte localization to the cortex versus medulla are largely conserved between humans and mice.

We also placed purified human fetal thymocytes on human thymic slices prepared from the same donor (Figure 1A). Isolated, mature $CD4^+$ and $CD8^+$ SP thymocytes added to slices localized preferentially to the medulla, mirroring their behavior on mouse thymic slices. Surprisingly, immature DN and DP human thymocyte populations did not localize preferentially to the cortex as they did on mouse slices, but rather displayed similar densities in the cortex and medulla of human thymic slices (Figure 1, E and F), despite the finding that cultured human thymic slices maintained cortical and medullary structure and showed appropriate localization of endogenous thymocytes to the cortex and medulla, as assessed by CD1a staining (Figure 1G). These observations suggest that human immature thymocytes are responsive to localization signals from the thymic stroma, but that these signals are not adequately provided by the human stroma in this model. Because endogenous DP human thymocytes retained their cortical localization within human slices (Figure 1G), this suggests a more stringent requirement for migration of ex vivo–isolated DP thymocytes to the cortex after addition to slices.

Next, we examined the migration characteristics of human thymocytes within thymic slices using 2-photon microscopy. Immature DN and DP thymocytes in the cortical region of mouse thymic slices migrated with speeds of approximately 4 μm/min, similar to previous reports for mouse cortical DN and polyclonal DP thymocytes from both intact and vibratome-cut thymic lobes (27, 29, 30). Mature human $CD4^+$ and $CD8^+$ SP thymocytes in the medulla migrated more rapidly than did immature cells in the cortex, exhibiting average speeds of approximately 9 and 12 μm/min, respectively (Figure 2, A and B, and Supplemental Video 1; supplemental material available online with this article; doi:10.1172/JCI67175DS1). Remarkably, these values were in close agreement with previous reports of mouse $CD4^+$ and $CD8^+$ SP thymocytes (~9–16 μm/min) as well as with reported mature $CD4^+$ and $CD8^+$ T cell speeds in lymph nodes (~10–13 μm/min) (8, 27, 31, 32). We noted that the few $CD8^+$ SP cells found in the cortex migrated rapidly and displayed an average speed of approximately 10 μm/min (Figure 2B), which suggests that the developmental state of the cell, rather than differences in cortical versus medullary environment, represents the major factor determining human thymocyte

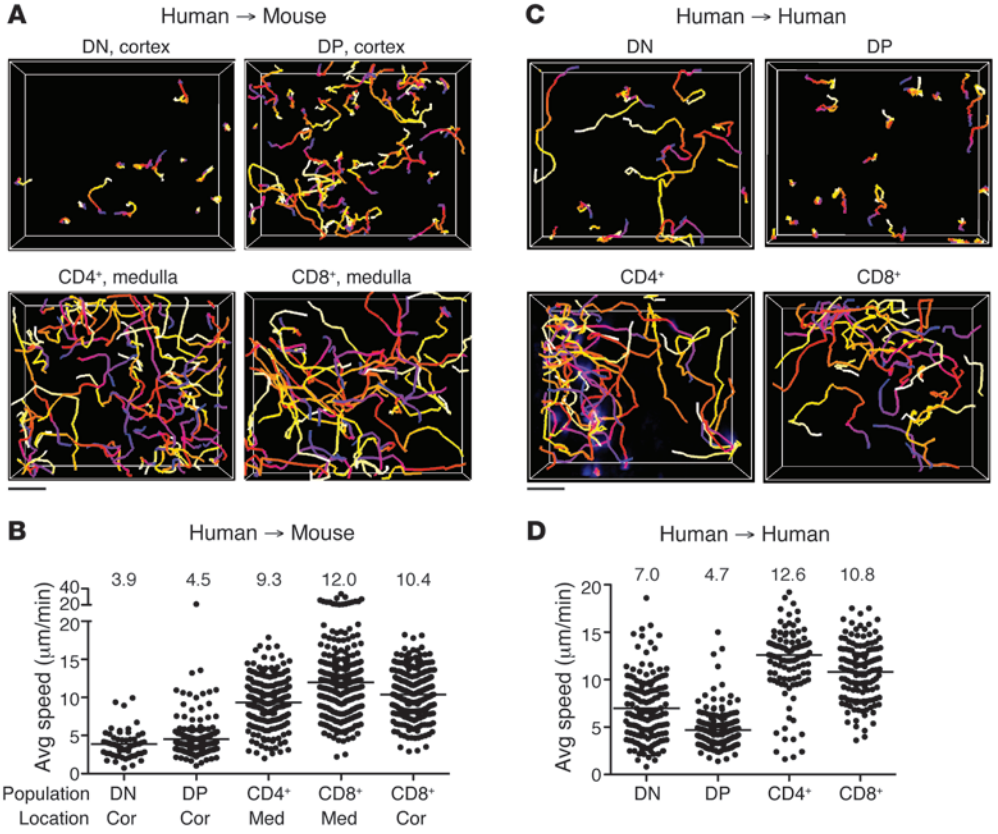

Figure 2

Human and mouse thymic slices support human thymocyte migration. (**A**) Cell tracks from representative 2-photon time-lapse datasets of human thymocyte subsets on CD11c-YFP thymic slices (20-minute movies). (**B**) Average speed of human thymocytes on CD11c-YFP thymic slices. $CD4^+$ and $CD8^+$ SP movies were acquired in the medulla (med) or cortex (cor); DN and DP movies were acquired in the cortex. n = 57 tracks (DN); 178 tracks (DP); 207 tracks ($CD4^+$); 274 tracks ($CD8^+$ in medulla); 279 tracks ($CD8^+$ in cortex). (**C**) Cell tracks from representative 2-photon time-lapse movies of human thymocyte subsets on human thymic slices (30-minute movies). (**D**) Average speed of human thymocytes on human thymic slices. n = 151 tracks (DN); 187 tracks (DP); 107 tracks ($CD4^+$); 135 tracks ($CD8^+$). (**A** and **C**) Tracks are color-coded to indicate passage of time (blue→red→yellow→white). (**B** and **D**) Symbols represent average speed of individual tracked cells; lines represent average value of compiled track averages for each population. Scale bars: 30 μm.

motility. To examine human thymocyte migration on human stroma, we relied on relative density of labeled thymocytes to distinguish cortex versus medulla during imaging, and are therefore less confident about assigning individual imaging volumes to cortex or medulla. Nevertheless, we consistently observed that SP thymocytes migrated more rapidly than did DP thymocytes (Figure 2, C and D, and Supplemental Video 1). The average speed of DN cells on human slices was more heterogeneous than that on mouse slices, and DN cells had higher motility on human versus mouse slices (average speed, 7 vs. ~4 μm/min). Even so, human DN cells were substantially slower than human SP cells on human thymic slices. Together, these data showed that the motility of human thymocytes on mouse slices was similar to that on human slices and validated the interspecies thymic slice model as a means to elucidate the molecular signals involved in human thymocyte migration.

Interactions with MHC on mouse stroma sustain the activation and motility of human DP thymocytes. Although positive selection is thought to require specific recognition of peptide-MHC complexes on thymic stromal cells, there are also indications that a large proportion of DP thymocytes receive low-level TCR signals from MHC recognition, leading to upregulation of activation markers and maintenance of basal motility in the thymic cortex (29, 33, 34). To determine whether mouse MHC can provide these signals to human thymocytes, we cultured DP human thymocytes on thymic lobes of mice deficient in MHC classes I and II (referred to herein as MHC-deficient mice) or WT mice for 72 hours, and then examined expression of CD69 and CD5 as indicators of TCR engagement of MHC (33). Human thymocytes recovered from WT, but not MHC-deficient, thymic slices showed upregulation of both CD69 and CD5, reflected as a shift in the overall mean fluorescence intensity on the DP population, and an increase in the proportion of $CD69^{hi}$ cells (Figure 3, A–D). We also compared the speeds of human DP cells in the cortex of MHC-deficient versus WT thymic slices. Human DP motility was significantly reduced on MHC-deficient versus WT thymic slices (~3.0 vs. ~4.4 μm/min; Figure 3, E and F). In contrast, the speed of mature $CD8^+$ SP thymocytes was similar on thymic slices of WT mice and mice deficient in MHC class I only (Figure 3, G and H). These data indicated that mouse MHC can engage human thymocytes and thereby contribute to the maintenance of human DP thymocyte motility.

Changes in chemokine responsiveness at the DP-to-SP transition. Chemokines are likely candidates to play a role in the migration and localization of human thymocytes. Although numerous studies have examined chemokine receptor expression and chemokine responsiveness of postnatal human thymocytes, there is limited information regarding chemokine responsiveness of human fetal thymocytes (11). We therefore used flow cytometric analysis to examine human fetal thymocytes for their expression of CCR7 and CXCR4, 2 chemokine receptors whose ligands are differentially expressed in the cortex versus the medulla (9). CCR7, the receptor for the medullary chemokine CCL21, was upregulated on both $CD4^+$ and $CD8^+$ SP thymocytes, with the highest levels seen on the more mature $CD1a^-$ SP cells (Figure 4A). DP thymocytes were low for CCR7, although some expression was detected on the TCR-signaled $CD69^+$ DP thymocytes, in line with previous reports from mouse adult thymocytes (10, 35). In contrast, CXCR4, the receptor for the cortical chemokine CXCL12, was

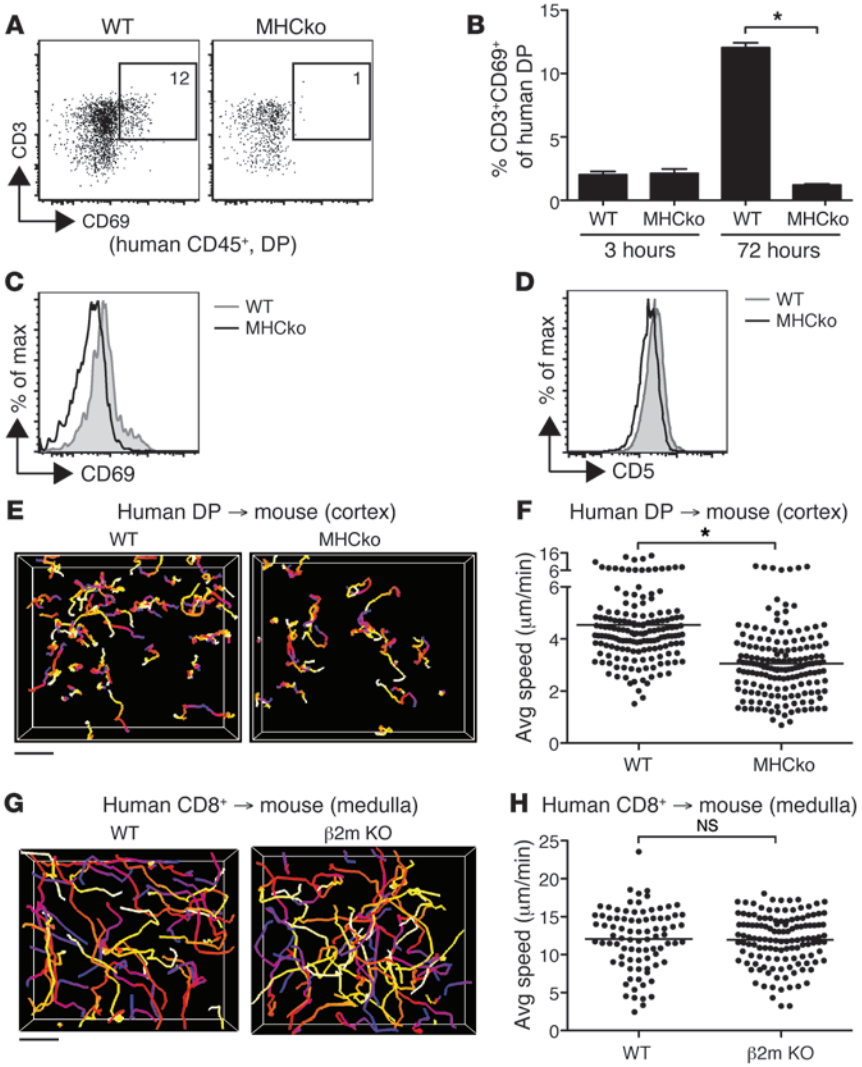

Figure 3
Interspecies recognition of MHC affects activation and motility of immature human thymocytes on mouse stroma. (**A**) Flow cytometric analysis of WT or MHC-deficient (MHCko) thymic slices overlaid with enriched DP cells and harvested after 72 hours. Representative analysis of CD3 and CD69 on DP cells is shown. (**B**) CD69 upregulation on $CD3^+$ DP cells at 3 and 72 hours after initiation of culture on mouse thymic slices. Bars indicate mean ± SEM of 3 different slices per genotype from 1 representative experiment of 2. (**C** and **D**) Overall expression levels of (**C**) CD69 and (**D**) CD5 on DP thymocytes 72 hours after culture on mouse WT or MHC-deficient slices. Representative of 2 independent experiments run in triplicate. (**E**) Cell tracks from representative 2-photon time-lapse datasets of DP cells in the cortex of WT or MHC-deficient CD11c-YFP slices (20-minute movies). (**F**) Average speed of DP cells in the cortex of WT (n = 161 tracks) or MHC-deficient (n = 169 tracks) CD11c-YFP slices. (**G**) Cell tracks from representative 2-photon time-lapse datasets of $CD8^+$ SP cells in the medulla of WT or MHC class I–deficient (β2m KO) CD11c-YFP slices (20-minute movies). (**H**) Average speed of $CD8^+$ SP cells in the medulla of WT (n = 144 tracks) or MHC class I–deficient (n = 270 tracks) CD11c-YFP slices. (**E**–**H**) Track color-coding, symbols, and lines as in Figure 2. Scale bars: 30 μm. $^*P < 0.05$.

expressed at higher levels on DP compared with SP thymocytes, with the TCR-signaled $CD69^+$ DP thymocytes expressing lower levels than $CD69^-$ DP thymocytes (Figure 4B).

The surface expression of CCR7 and CXCR4 on human fetal thymocyte subsets closely corresponded to their in vitro chemokine responsiveness, as measured by transwell migration assays (Figure 4, C–E). Responsiveness to CCL21 increased with increasing maturation state, with DP thymocytes showing very little response and the most mature SP thymocytes migrating robustly (Figure 4C). In contrast, a strong response to CXCL12 was observed with $CD69^-$ DP thymocytes, with a markedly reduced response after positive selection in $CD69^+$ DP and $CD1a^+$ SP populations (Figure 4D). These data — in agreement with previous reports for postnatal thymocytes (11, 36) — indicate that positive selection signals at the DP stage are accompanied by a change in responsiveness to both CCL21 and CXCL12. Interestingly, chemotaxis toward CXCL12 was regained in the most mature $CD8^+$ SP thymocytes (Figure 4D), consistent with murine and human studies that suggest a role for CXCR4 in thymic egress (37, 38). We also examined responses of human fetal thymocytes to another cortical chemokine, CCL25, and found that all subsets exhibited robust migration toward CCL25, with no apparent difference between $CD69^-$ and $CD69^+$ DP thymocytes (Figure 4E). It is also noteworthy that similar chemotactic responses were observed with human and mouse chemokines (Figure 4, C–E), further validating the use of the interspecies thymic slice model as an experimental system to probe human thymocyte localization and migration.

CCR7 signaling directs the appropriate intrathymic localization of human $CD8^+$ SP thymocytes. To test the role of chemokine receptors on human thymocyte migration in situ, we examined the effect of pertussis toxin (PTX), which blocks signaling through chemokine and other GPCRs. Treatment of $CD8^+$ SP thymocytes with PTX just prior to seeding onto human thymic slices abolished their preferential localization to the medulla (Figure 5, A and B). This effect corresponded with a drop in $CD8^+$ SP speed in the medulla of murine slices (from ~12 to ~8 μm/min) and was also confirmed on human thymic slices (from ~11 to ~7 μm/min) (Figure 5, C–F, and Supplemental Video 2). The observed effect of PTX treatment on the speed of SP thymocytes agrees with data from mouse studies and indicates that GPCR signaling helps to promote mature SP thymocyte motility and localization to the thymic medulla (8).

Mature SP human thymocytes migrated in response to CCR7 ligands in vitro (Figure 4C), and previous mouse studies have shown that CCR7 is essential for directing SP thymocytes to the

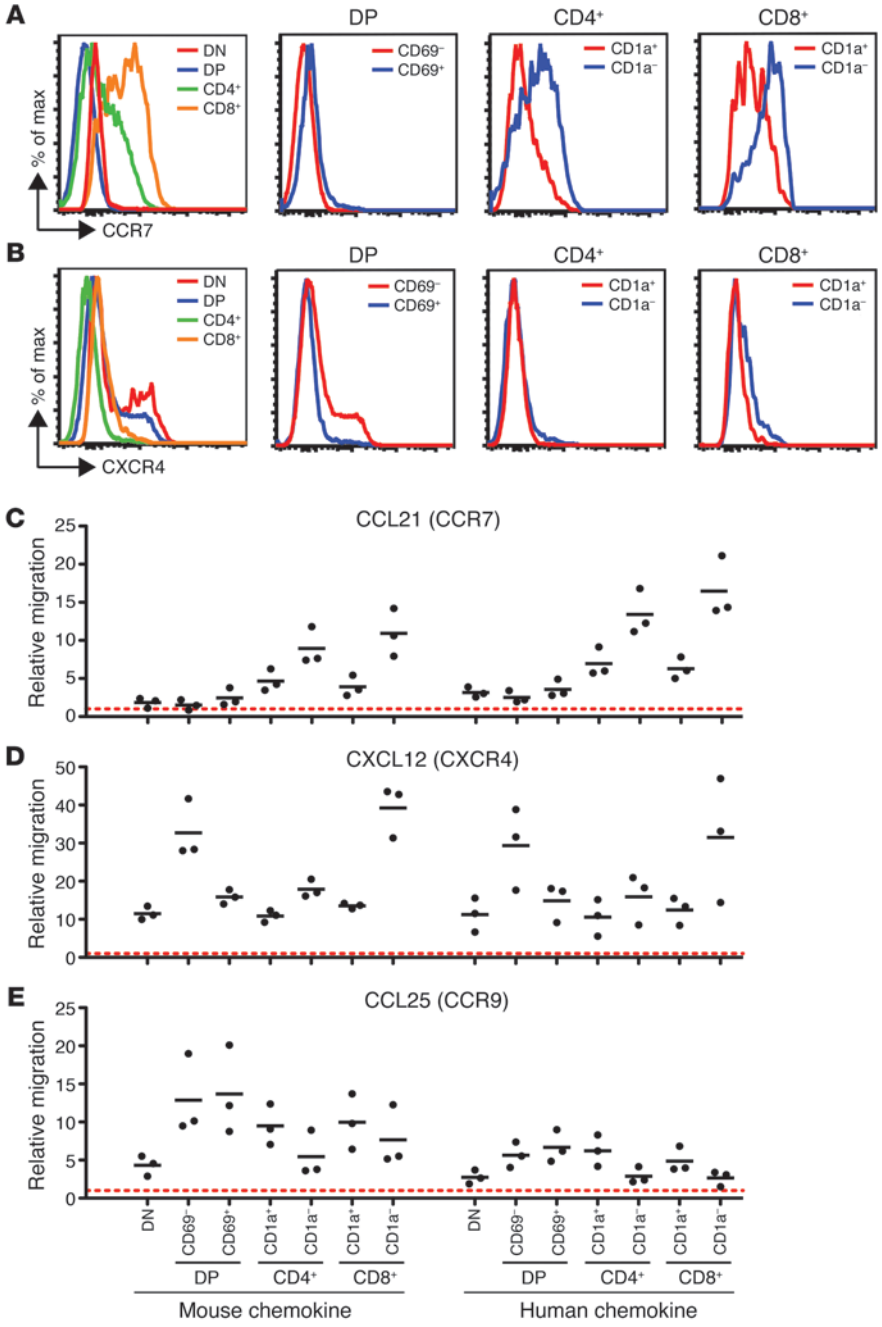

Figure 4
Developmentally regulated chemokine receptor expression and migration in human thymocytes. (**A** and **B**) Relative levels of (**A**) CXCR4 and (**B**) CCR7 expression on the indicated gated populations of human fetal thymocytes, as assessed by flow cytometry. (**C**–**E**) Relative migration of human thymocyte populations toward mouse and human chemokines, as assessed by transwell assay. Migration was normalized to no-chemokine controls (dashed red lines). Experiments were performed twice with similar results; a representative experiment is shown.

medulla (7, 8, 39). To determine whether CCR7 signaling is also necessary for the localization of mature human SP thymocytes to the medulla, we examined SP localization on thymic slices from mice lacking CCR7 ligands (*plt/plt* mice) (40). The lack of CCR7 ligands disrupted localization of $CD4^+$ and $CD8^+$ SP thymocytes and led to similar densities in the cortex and medulla, mirroring the effect of PTX-treated $CD8^+$ SP thymocytes on human thymic slices. In contrast, the preferential segregation of DP thymocytes to the cortex was preserved in thymic slices from *plt/plt* mice (Figure 5, G and H). Thus, CCR7 appears to be a key GPCR responsible for directing both human and mouse SP thymocytes to the medulla, but does not have a major effect on the localization of DP thymocytes in the cortex.

CXCR4 signaling retains human DP thymocytes in the thymic cortex. To explore the contribution of chemokines to the cortical segregation of immature human thymocytes, we examined the effect of PTX treatment on the intrathymic localization of human DP thymocytes. PTX-treated DP thymocytes seeded onto mouse thymic slices no longer displayed preferential accumulation to the cortex, but were distributed equally between cortical and medullary compartments (Figure 6, A and B). We also examined the effect of PTX treatment on the speed of DP thymocytes in the cortex using 2-photon time-lapse microscopy. PTX treatment had a modest effect on the speed of DP thymocytes in the cortex of mouse thymic slices (from ~4.5 to ~4 μm/min) and no significant effect on human thymic slices (Figure 6, C and D). These data indicate

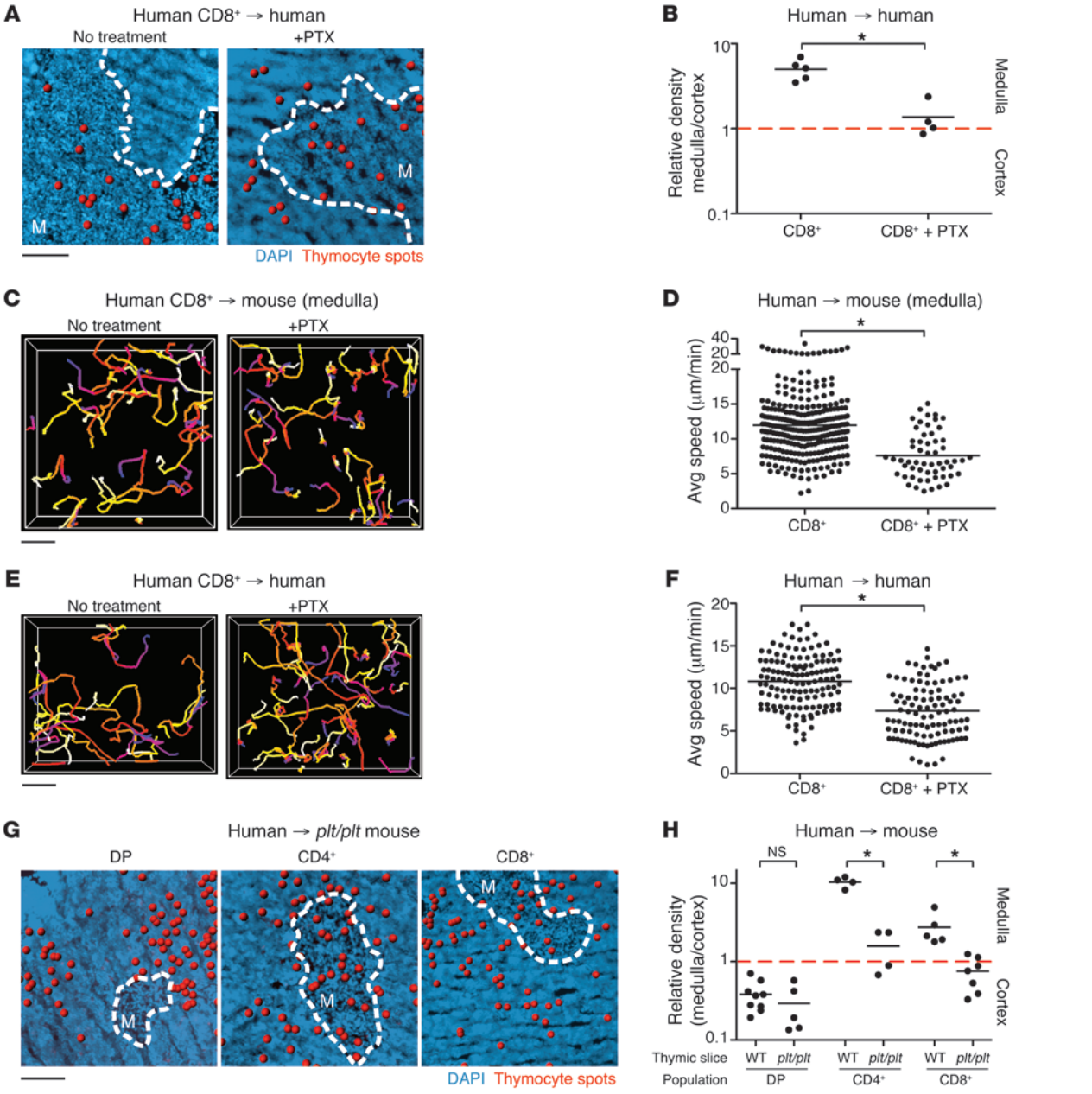

Figure 5

CCR7 signaling directs intrathymic localization of human CD8+ SP thymocytes. (**A**) Representative fixed cryosections of untreated and PTX-treated CD8+ SP human thymocytes overlaid on human thymic slices. (**B**) Relative density of PTX-treated CD8+ SP cells on human thymic slices. Data were compiled from at least 3 tissue sections from at least 2 independent experiments. *n* = 265 cells. Untreated CD8+ SP cells from Figure 1F are shown for comparison. (**C**) Cell tracks from representative 2-photon time-lapse datasets of untreated or PTX-treated CD8+ SP cells on CD11c-YFP thymic slices imaged in the medulla (20-minute movies). (**D**) Average speed of PTX-treated CD8+ SP cells in the medulla of CD11c-YFP thymic slices. Data were compiled from a minimum of 2 different imaging volumes from at least 2 experiments. *n* = 57 tracks. Untreated CD8+ SP cells from Figure 2B are shown for comparison. (**E**) Cell tracks from representative 2-photon time-lapse datasets of untreated or PTX-treated CD8+ SP cells on human thymic slices (30-minute movies). (**F**) Average speed of PTX-treated CD8+ SP cells on human thymic slices. *n* = 105 tracks. Untreated CD8+ SP cells from Figure 2D are shown for comparison. (**G**) Representative fixed cryosections of human thymocyte subsets overlaid on *plt/plt* thymic slices. (**H**) Relative density of each human thymic subset on *plt/plt* thymic slices. *n* = 2,210 cells (DP); 1,435 cells (CD4+); 8,271 cells (CD8+). Thymocyte subsets on WT slices from Figure 1D are shown for comparison. (**A** and **G**) Dashed outlines as in Figure 1. (**B** and **H**) Each dot represents quantification of 1 tissue section. (**C**–**F**) Track color-coding, symbols, and lines as in Figure 2. Scale bars: 100 μm (**A** and **G**); 30 μm (**C** and **E**). *$P < 0.05$.

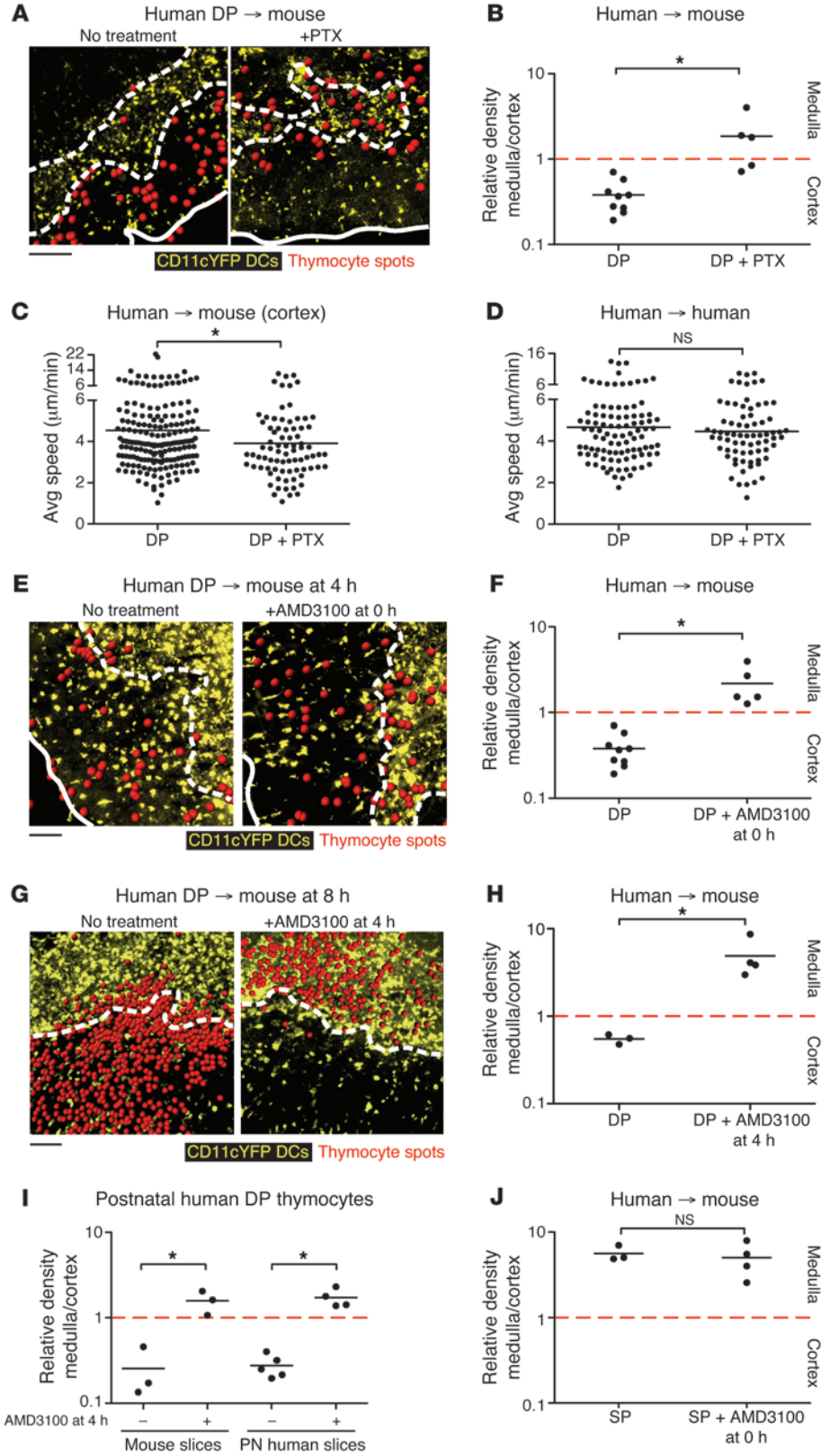

Figure 6

CXCR4 directs the appropriate localization of human DP thymocytes. (**A** and **B**) Representative cryosections (**A**) and relative density (**B**) of untreated (from Figure 1D) and PTX-treated (n = 358) fetal DP thymocytes on CD11c-YFP slices. (**C** and **D**) Average speed of (**C**) untreated (from Figure 2B) or PTX-treated (n = 80) fetal DP cells in the cortex of CD11c-YFP slices and on (**D**) human fetal thymic slices. n = 97 (DP); 73 (DP+PTX). (**E** and **F**) Fetal DP thymocytes were incubated with AMD3100 at the start of culture, and their location was determined after 4 hours. Representative cryosections (**E**) and relative density (**F**) of untreated (n = 5,282) or AMD3100-treated (n = 1,530) fetal DP thymocytes on CD11c-YFP slices. (**I**) Postnatal (PN) DP thymocytes were overlaid onto CD11c-YFP or human postnatal slices for 4 hours, washed, then treated or not with AMD3100 for another 4 hours. n = 1,006 (mouse DP); 2,221 (mouse DP+AMD3100); 2,752 (postnatal human DP); 1,308 (postnatal human DP+AMD3100). (**J**) Relative density of untreated (n = 1,392) or AMD3100-treated (n = 1,605) fetal $CD4^+$ and $CD8^+$ SP thymocytes on CD11c-YFP slices. Data were compiled from at least 3 tissue sections from at least 2 independent experiments. (**A**, **E**, and **G**) Solid and dashed outlines as in Figure 1. (**C** and **D**) Symbols and lines as in Figure 2. (**B**, **F**, and **H**–**J**) Each dot represents quantification of 1 tissue section. Scale bars: 100 μm. *$P < 0.05$.

that GPCR signaling helps to direct the localization of human DP thymocytes within the thymus, but does not have a major effect on their overall motility.

We next tested whether CXCR4 is the GPCR responsible for the cortical localization of DP thymocytes, using the CXCR4 small-molecule inhibitor AMD3100 (40). We first confirmed the specificity of AMD3100 for CXCR4 using transwell migration assays (Supplemental Figure 1). As expected, AMD3100 strongly inhibited the in vitro migration of human fetal thymocytes to both human and murine CXCL12, but did not affect their migration to CCL25 or CCL21. We then tested the effect of the drug on the localization of human thymocytes on mouse thymic slices. We found that DP cells treated with AMD3100 no longer segregated to the cortex and, in fact, displayed a slight medullary bias (Figure 6, E and F). In contrast, AMD3100 treatment had no significant effect on mature SP thymocyte localization to the medulla (Figure 6J).

The effect of AMD3100 treatment on DP localization suggested that CXCR4 signaling is needed to attract DP thymocytes to the cortex and prevent them from prematurely migrating from the cortex to the medulla. However, an alternative possibility was that the drug affects the ability of DP thymocytes to enter the cortex or medulla from the surface after seeding onto the thymic slice. To distinguish between these possibilities, we first allowed human DP thymocytes to migrate into the tissue for 4 hours in the absence of the drug, and then added AMD3100 and continued culturing the slices for another 4 hours prior to analysis. Under these conditions, entry of DP thymocytes into the thymic slice was more efficient (data not shown), perhaps due to the longer time allowed for migration. More importantly, addition of AMD3100 to thymic slices after human DP thymocytes had localized to the cortex led to a striking relocalization to the medulla (Figure 6, G and H).

We also tested the effect of AMD3100 on the localization of human thymocytes on human thymic slices. For this experiment, we used human postnatal DP thymocytes and thymic slices, which, unlike fetal thymus samples (Figure 1F), exhibited appropriate accumulation of DP thymocytes in the cortex (Figure 6I). We allowed postnatal DP thymocytes to migrate into either postnatal human or mouse thymic tissue for 4 hours and then added AMD3100 and continued culturing the slices for a total of 8 hours. Addition of AMD3100 inhibited the cortical segregation of postnatal human DP thymocytes on both mouse and human postnatal thymic slices (Figure 6I). These data implicate CXCR4 as a critical mediator in the localization of human DP cells, supporting a chemoattractant role for CXCL12 in both directing and retaining human DP thymocytes to the thymic cortex.

Discussion

Our current understanding of human thymocyte migration is based largely on in vitro chemokine migration data and extrapolation from studies in mice; thus, the signals that control human thymocyte migration in vivo are not known. Here, we directly examined the intrathymic migration patterns of human thymocytes on both mouse and human thymic stroma and investigated the effect of TCR and chemokine signals on these patterns. Our findings revealed some notable similarities between humans and mice, including the role of the CCR7-CCL19/21 axis in attracting mature SP thymocytes to the medulla. We also revealed a role of the CXCR4-CXCL12 axis in retaining immature DP thymocytes in the cortex. These data provide the first evidence that 2 opposing chemokine gradients control the migration of thymocytes from the cortex to the medulla at the DP-to-SP developmental checkpoint and indicate a striking degree of interspecies crosstalk between human thymocytes and mouse thymic stroma.

The prevailing view of chemokine signaling during T cell development holds that chemokines play little role in the thymic cortex (2, 8). This notion is based in part on the relative dearth of chemokine expression in the cortex compared with the medulla and the subcapsular zone (9). In addition, the in vitro responsiveness of mouse DP thymocytes to cortical chemokines is dampened by expression of the adaptor protein GIT2 and the glycoprotein PlexinD1 (15, 16). Moreover, mice bearing mutations in receptors for the 2 known cortical chemokines, CXCR4 and CCR9, did not display clear phenotypes at the DP stage, although defects at early stages of thymic development were previously noted (12–14, 41–43). In sharp contrast to this view, we saw a striking effect of CXCR4 inhibition on human DP thymocyte localization within the thymus. Moreover, there was marked downregulation of CXCR4 expression and a decrease in CXCL12 responsiveness in $CD69^+$ DP and SP human fetal thymocytes compared with $CD69^-$ DP cells. In contrast, responsiveness to CCL25 did not show substantial variation among the different human thymocyte populations. Although CXCL12 is required for DP thymocytes to accumulate in the cortex, chemokine signaling itself may also affect expression and activation of adhesion molecules such as integrins, which in turn may contribute to the ability of DP thymocytes to migrate on cortical, but not medullary, stroma (8, 44, 45). These data fit with the view that DP thymocytes undergoing positive selection respond to 2 competing chemokine gradients: one emanating from the cortex, dominated by the CXCR4/CXCL12 axis, and one from the medulla, dominated by the CCR7-CCL19/21 axis. Prior to positive selection, the CXCR4 signal predominates, helping to retain DP thymocytes in the cortex. However, as thymocytes mature in response to positive selecting signals, they downregulate CXCR4 and upregulate CCR7, thereby promoting migration from the cortex to the medulla.

While our results point to an important role for CXCR4 in actively retaining DP thymocytes in the cortex, we did not observe a major effect of the global chemokine receptor inhibitor PTX on the overall motility of human DP thymocytes. In fact, as reported here and shown previously with mouse thymocytes (8, 27, 29), cortical thymocytes were more than 2-fold slower than their medullary counterparts. Moreover, we found that PTX treatment sharply reduced the speed of human SP thymocytes, but had a minor effect on DP thymocyte speed. These data suggest that the relatively slow migration of human DP thymocytes may be determined by other factors, such as altered integrin activation, rather than by chemokine signaling (44, 45).

Previous studies using mouse thymocytes and mature T cells revealed a context-dependent effect of TCR signaling on motility. TCR signaling can promote migration, as in the requirement for tonic MHC signals to sustain the motility of the bulk of DP thymocytes within the cortex and the rapid directional migration toward the medulla associated with positive selection (29, 30). In other contexts, TCR signaling can lead to reduced motility, such as the brief periods of migratory arrest triggered by positive selection and slowing of SP thymocytes due to encounters with high-avidity self-antigens in the thymic medulla (25, 27). Likewise, mature naive T cells typically undergo migratory arrest upon initial encounter with antigen-loaded DCs, but eventually recover their motility (32, 46–48). Our current observation of enhanced

motility of polyclonal human DP thymocytes in the presence of mouse MHC is fully compatible with these previous studies and supports the notion that tonic TCR signals promote immature thymocyte migration in the cortex.

Humanized mice, in which human thymocytes develop in contact with mouse thymic stroma, are important models for human immune development and function, but how human T cells are selected in these systems is not well understood (20, 22). Human CD8 and CD4 can interact with mouse MHC class I and MHC class II, respectively, and there are indications that human thymocytes can undergo positive selection on mouse MHC (21–23, 49–51). However, human thymocytes express both MHC class I and MHC class II, and there is evidence that some positive selection in humanized mice occurs via human thymocyte-thymocyte interactions (52). Thus, it is unclear whether interactions between human thymocytes and mouse stromal cells are extensive and productive, or whether only rare human thymocytes can cross-react with mouse MHC. Here we provided evidence that the bulk of human DP thymocytes can receive MHC-dependent signals from mouse thymic stroma that sustain their motility and activation state, an effect that was mediated by human TCR and/or $CD4^+$ and $CD8^+$ coreceptors binding to mouse MHC. These data point to a surprising degree of interspecies conservation in thymocyte-stromal interactions between humans and mice and suggest that selection of human thymocytes by murine stromal elements may be quite efficient.

Our study presented 2 complementary models to examine human thymocyte migration within a living 3-dimensional thymic stromal environment: the human→mouse system allowed for manipulation of stromal cell environments using genetically engineered mice, and the human→human system provided information about the human thymic microenvironment. Together, these systems offer a unique opportunity to study the molecular signals that direct human T cell behavior and development, as well as interspecies crosstalk, and should help to inform the development of improved in vivo humanized mouse models. Moreover, immune-modulatory drugs, including small-molecule antagonists to chemokine receptors, such as AMD3100, represent an emerging therapeutic modality (53). We foresee that the thymic slice model may serve as a preclinical tool to investigate the effect of immune-modulatory drugs on human thymocyte development. This tool may be of particular relevance to the treatment of infants and children, whose peripheral T cell pool is predominantly shaped by recent thymic emigrants.

Methods

Human thymocyte subset purification. Consent for and procurement of human fetal thymic tissue (18–20 weeks) was provided by Advanced Bioscience Resources in accordance with federal, state, and local law. Postnatal thymi were obtained as a surgical byproduct during corrective cardiac surgery in pediatric patients 1 week to 2 years of age in accordance with the ethics review committee of Children's Hospital and Research Center Oakland. Thymic tissue was dissociated into a single-cell suspension using a glass tissue homogenizer. Each experimental replicate was obtained from tissue from a single sample, and each experiment was performed at least 2 times with independent human thymic tissue. A total of 49 individual thymic samples were obtained for this study, of which 3 samples were excluded due to poor cell yield. Thymocyte subsets were negatively enriched using the EasySep Biotin Positive Selection Kit for depletion, as directed by the manufacturer (STEMCELL Technologies). Thymocytes were incubated with human Fc block, and all subsets were depleted for non–T cell lineages using anti-human CD11c, CD14, CD16, CD19, CD20, CD123, and CD235a (eBioscience) and CD56 (BD Biosciences) antibodies conjugated to biotin. Additional biotinylated antibodies were added as follows for enrichment of thymic subsets: DN, anti-human CD4 (clone OKT4), CD8 (clone HIT8a), and CD3; preselection DP, anti-human CD69 and CD34; $CD4^+$ SP, anti-human CD8 (clone HIT8a), CD1a, and CD34; $CD8^+$ SP, anti-human CD4 (clone OKT4), CD1a, and CD34; mature SP ($CD4^+$ and $CD8^+$ together), anti-human CD1a and CD34 (eBioscience).

Flow cytometry. Pre- and postenrichment thymocytes or single-cell suspensions from thymic slices were stained with anti-human CD1a-PE, CD3–APC-eFluor 780, CD4–APC-eFluor 780 (clone RPA-T4), CD4–eFluor 450 (clone RPA-T4), CD8a–PE-Cy7 (clone RPA-T8), CD7–PE-Cy5, CD45–PerCP-Cy5.5, CD69-biotin, TCRαβ-FITC, CXCR4-APC, and CCR7-APC antibodies as well as streptavidin–Pacific Blue or streptavidin-APC (eBioscience). Cells were incubated with antibody for 20 minutes at 4°C, except for staining for CCR7 (1 hour at 37°C). Samples were run on an LSRII flow cytometer (BD Biosciences), and data were analyzed with FlowJo software (Tree Star).

Thymocyte labeling and treatment. Single-cell thymocyte suspensions were resuspended at 1×10^7 cells/ml in PBS and labeled with a final concentration of 2 μM SNARF-1 or 0.5 μM CFDA-SE (Invitrogen) for 10 minutes at 37°C. Cells were washed 3 times with complete DMEM and treated or directly applied to thymic slices. PTX-treated thymocytes were incubated with 100 ng/ml PTX (Sigma-Aldrich) for 10 minutes at 37°C in complete DMEM, then washed 3 times in complete DMEM. The activity of each lot of PTX was confirmed. AMD3100-treated DP or SP thymocytes were resuspended in 1 μg/ml AMD3100 (Sigma-Aldrich) in complete DMEM during migration into the slice and underneath the transwell. In some experiments, AMD3100 was added to the slices briefly (5–10 minutes) and to the media underneath the transwell after the thymocytes had migrated into the tissue for 4 hours.

Mice. Mice were housed and bred at the American Association of Laboratory Animal Care–approved facility at the Life Sciences Addition at UC Berkeley under pathogen-free conditions. Experiments were approved by the Animal Care and Use Committee. C57BL/6 and CD11c-YFP mice were bred in house (28). MHC class I–knockout (β2m) and MHC-deficient (Abb-β2m) mice were obtained from Taconic and bred with CD11c-YFP transgenic mice (54). CCL19 and CCL21a mutant (*plt/plt*) mice on the C57BL/6 background were purchased from The Jackson Laboratory (40).

Thymic slices. Mouse and human thymic slices were prepared essentially as described previously (55). For mouse tissue, individual thymic lobes were embedded in 4% low-melt agarose dissolved in HBSS. For human tissue, a portion of the thymic tissue was removed using a scalpel and embedded in the agarose solution. Tissue slices were cut to a thickness of 500 μm using a Vibratome 1000 Plus Sectioning System and feather blades (Leica Microsystems), then transferred to a 0.4-μm organotypic cell culture insert (BD Biosciences) over 1.5 ml complete DMEM in a 6-well plate. Excess liquid was removed from the tissue slice by pipetting, and $0.5–2 \times 10^6$ cells were overlaid in 10 μl complete DMEM. Thymocytes were allowed to migrate into the slice for 2–4 hours in a 37°C incubator, and cells remaining outside the tissue were washed by indirect pipetting of media over the slice.

2-photon imaging. Thymic slices were glued to a coverslip (3M Vetbond tissue glue adhesive) and maintained in 37°C, oxygenated phenol red–free DMEM. Fluorescent cells within the thymic slices were imaged using 2-photon microscopy using either a custom-built 2-photon microscope with a Spectra-Physics MaiTai Laser (×20/0.95 Nikon objective) or a Zeiss 7 MP microscope (×20/1.0 Zeiss objective) with a Coherent Chameleon laser tuned to 920 nm. Second harmonics, CFDA-SE/YFP, and SNARF were separated with 495 nm, 560 nm, and 650 nm dichroic mirrors, respectively, and a 450 nm/80 nm bandpass filter on the custom-built 2-photon

microscope, or CFDA-SE/YFP and SNARF were separated on the Zeiss 510 microscope using a 560-nm dichroic mirror. Image areas of 172 × 143 μm (custom) or 175 × 175 μm (Zeiss) were scanned every 30 seconds for 20–30 minutes, with 3-μm *z* steps taken from beneath the cut site and up to 150 μm below the cut surface, using custom or ZEN software, respectively.

Immunofluorescence microscopy. Thymic slices were fixed in 4% formaldehyde for 5 minutes and subsequently passed through a sucrose gradient prior to embedding in OCT. Embedded slices were frozen over dry ice and then stored at –80°C. 10-μm frozen sections were cut using a HM550 OMVP cryostat (ThermoScientific) and stored at –80°C. Sections were fixed in acetone for 10 minutes at –20°C, rehydrated in PBS for 10 minutes, and then stained with DAPI. Human slides were stained with purified CD1a (clone HI149; eBioscience) overnight at 4°C, biotin-labeled goat anti-mouse IgG (BD Bioscience) for 1 hour at room temperature, and then streptavidin–Alexa Fluor 488 (Invitrogen) for 30 minutes at room temperature. Coverslips were mounted on slides with Vectashield Mounting Medium for Fluorescence (Vector Laboratories). Images were captured using a Nikon TE2000 inverted or Nikon Eclipse E800 upright microscope with ×10/0.30 Nikon air objectives; images were acquired using NIS Elements AR or Slidebook software, respectively.

Chemotaxis assays. Human thymocytes were incubated in the presence or absence of 1 μg/ml AMD3100 (Sigma-Aldrich) for 30 minutes prior to applying 0.5×10^6 cells atop 5-μm transwell filters (Fisher) for 4 hours in wells containing medium alone or mouse or human chemokines. CCL25 (R&D Systems) and CCL21 (Peprotech) were used at a concentration of 1,000 ng/ml, and CXCL12 (Peprotech) at 100 ng/ml, concentrations that we have previously identified as providing optimal migration of human thymocytes. After 4 hours, cells from the bottom well were counted, stained with fluorescent antibodies, and analyzed by flow cytometry. Data are expressed as the number of migrated cells relative to no-chemokine control wells. Transwell assays were performed in triplicate from 2 independent samples.

Image analysis and statistics. Image analysis was carried out using standard and custom-written MATLAB scripts (Mathworks), Image J and Imaris (Bitplane Scientific Software), and Excel. The relative density of individual subsets was calculated by measuring the areas of cortex and medulla within each slice, counting the number of thymocytes within each area, and then normalizing as the ratio of medulla to cortex area. Data for each thymocyte subset were compiled from at least 4 tissue sections from a minimum of 2 independent experiments, and thymocyte speed data were compiled from a minimum of 3 different imaging volumes from at least 2 experiments, unless otherwise indicated in the figure legends. Graphing and statistical analysis was done using GraphPad Prism. A P value less than 0.05 was considered significant.

Study approval. Consent for and procurement of 18- to 20-week human fetal thymus tissue was provided by Advanced Bioscience Resources in accordance with federal, state, and local law. Postnatal thymi were obtained as a surgical byproduct during corrective cardiac surgery in pediatric patients 1 week to 2 years of age in accordance with the ethics review committee of Children's Hospital and Research Center Oakland. Mice were housed and bred at the American Association of Laboratory Animal Care–approved facility at the Life Sciences Addition at UC Berkeley under pathogen-free conditions. Experiments were approved by the Animal Care and Use Committee.

Acknowledgments

We thank B.J. Fowlkes, Lauren Ehrlich, Ena Ladi, Benjamin Haley, and members of the Robey and Winoto labs for critical reading of the manuscript and technical assistance. This work was supported by California Institute of Regenerative Medicine clinical fellowship TG2-01164 (to J. Halkias), postdoctoral training grant T1-00007 (to H.J. Melichar), graduate student training grant TG2-01164 (to J.O. Ross), a Shared Instrumentation Grant from the NIH (1S10RR026821), and grant RM1-01732 (to E.A. Robey) as well as by an undergraduate research award to B. Yen from private donations to the UC Berkeley Stem Cell Center.

Received for publication October 3, 2012, and accepted in revised form February 15, 2013.

Address correspondence to: Ellen Robey, UC Berkeley, Department of Molecular and Cell Biology, 142 Life Sciences Addition, #3200, Berkeley, California 94720-3200, USA. Phone: 510.642.8669; Fax: 510.643.9500; E-mail: erobey@berkeley.edu.

1. Ladi E, Yin X, Chtanova T, Robey EA. Thymic microenvironments for T cell differentiation and selection. *Nat Immunol*. 2006;7(4):338–343.
2. Love PE, Bhandoola A. Signal integration and crosstalk during thymocyte migration and emigration. *Nat Rev Immunol*. 2011;11(7):469–477.
3. Davalos-Misslitz AC, Worbs T, Willenzon S, Bernhardt G, Forster R. Impaired responsiveness to T-cell receptor stimulation and defective negative selection of thymocytes in CCR7-deficient mice. *Blood*. 2007;110(13):4351–4359.
4. Nitta T, Nitta S, Lei Y, Lipp M, Takahama Y. CCR7-mediated migration of developing thymocytes to the medulla is essential for negative selection to tissue-restricted antigens. *Proc Natl Acad Sci U S A*. 2009; 106(40):17129–17133.
5. Kurobe H, et al. CCR7-dependent cortex-to-medulla migration of positively selected thymocytes is essential for establishing central tolerance. *Immunity*. 2006;24(2):165–177.
6. Misslitz A, et al. Thymic T cell development and progenitor localization depend on CCR7. *J Exp Med*. 2004;200(4):481–491.
7. Ueno T, et al. CCR7 signals are essential for cortex-medulla migration of developing thymocytes. *J Exp Med*. 2004;200(4):493–505.
8. Ehrlich LI, Oh DY, Weissman IL, Lewis RS. Differential contribution of chemotaxis and substrate restriction to segregation of immature and mature thymocytes. *Immunity*. 2009;31(6):986–998.
9. Griffith AV, Fallahi M, Nakase H, Gosink M, Young B, Petrie HT. Spatial mapping of thymic stromal microenvironments reveals unique features influencing T lymphoid differentiation. *Immunity*. 2009; 31(6):999–1009.
10. Campbell JJ, Pan J, Butcher EC. Cutting edge: developmental switches in chemokine responses during T cell maturation. *J Immunol*. 1999;163(5):2353–2357.
11. Annunziato F, Romagnani P, Cosmi L, Lazzeri E, Romagnani S. Chemokines and lymphopoiesis in human thymus. *Trends Immunol*. 2001;22(5):277–281.
12. Plotkin J, Prockop SE, Lepique A, Petrie HT. Critical role for CXCR4 signaling in progenitor localization and T cell differentiation in the postnatal thymus. *J Immunol*. 2003;171(9):4521–4527.
13. Trampont PC, et al. CXCR4 acts as a costimulator during thymic beta-selection. *Nat Immunol*. 2010; 11(2):162–170.
14. Janas ML, Varano G, Gudmundsson K, Noda M, Nagasawa T, Turner M. Thymic development beyond beta-selection requires phosphatidylinositol 3-kinase activation by CXCR4. *J Exp Med*. 2010; 207(1):247–261.
15. Choi YI, et al. PlexinD1 glycoprotein controls migration of positively selected thymocytes into the medulla. *Immunity*. 2008;29(6):888–898.
16. Phee H, et al. Regulation of thymocyte positive selection and motility by GIT2. *Nat Immunol*. 2010; 11(6):503–511.
17. Lanier LL, Allison JP, Phillips JH. Correlation of cell surface antigen expression on human thymocytes by multi-color flow cytometric analysis: implications for differentiation. *J Immunol*. 1986; 137(8):2501–2507.
18. Lobach DF, Haynes BF. Ontogeny of the human thymus during fetal development. *J Clin Immunol*. 1987;7(2):81–97.
19. Spits H. Development of alphabeta T cells in the human thymus. *Nat Rev Immunol*. 2002; 2(10):760–772.
20. Shultz LD, Ishikawa F, Greiner DL. Humanized mice in translational biomedical research. *Nat Rev Immunol*. 2007;7(2):118–130.
21. Traggiai E, et al. Development of a human adaptive immune system in cord blood cell-transplanted mice. *Science*. 2004;304(5667):104–107.
22. Plum J, De Smedt M, Leclercq G, Taghon T, Kerre T, Vandekerckhove B. Human intrathymic development: a selective approach. *Semin Immunopathol*. 2008;30(4):411–423.
23. Strowig T, et al. Priming of protective T cell responses against virus-induced tumors in mice with human immune system components. *J Exp Med*. 2009; 206(6):1423–1434.
24. Huntington ND, et al. IL-15 transpresentation promotes both human T-cell reconstitution and T-cell-dependent antibody responses in vivo. *Proc*

Natl Acad Sci U S A. 2011;108(15):6217–6222.
25. Bhakta NR, Oh DY, Lewis RS. Calcium oscillations regulate thymocyte motility during positive selection in the three-dimensional thymic environment. *Nat Immunol*. 2005;6(2):143–151.
26. Fisher AG, Larsson L, Goff LK, Restall DE, Happerfield L, Merkenschlager M. Human thymocyte development in mouse organ cultures. *Int Immunol*. 1990;2(6):571–578.
27. Le Borgne M, et al. The impact of negative selection on thymocyte migration in the medulla. *Nat Immunol*. 2009;10(8):823–830.
28. Lindquist RL, et al. Visualizing dendritic cell networks in vivo. *Nat Immunol*. 2004;5(12):1243–1250.
29. Ladi E, et al. Thymocyte-dendritic cell interactions near sources of CCR7 ligands in the thymic cortex. *J Immunol*. 2008;181(10):7014–7023.
30. Witt CM, Raychaudhuri S, Schaefer B, Chakraborty AK, Robey EA. Directed migration of positively selected thymocytes visualized in real time. *PLoS Biol*. 2005;3(6):e160.
31. Bousso P, Robey EA. Dynamic behavior of T cells and thymocytes in lymphoid organs as revealed by two-photon microscopy. *Immunity*. 2004;21(3):349–355.
32. Miller MJ, Wei SH, Parker I, Cahalan MD. Two-photon imaging of lymphocyte motility and antigen response in intact lymph node. *Science*. 2002; 296(5574):1869–1873.
33. Azzam HS, Grinberg A, Lui K, Shen H, Shores EW, Love PE. CD5 expression is developmentally regulated by T cell receptor (TCR) signals and TCR avidity. *J Exp Med*. 1998;188(12):2301–2311.
34. Merkenschlager M, Graf D, Lovatt M, Bommhardt U, Zamoyska R, Fisher AG. How many thymocytes audition for selection? *J Exp Med*. 1997; 186(7):1149–1158.
35. Yin X, et al. CCR7 expression in developing thymocytes is linked to the CD4 versus CD8 lineage decision. *J Immunol*. 2007;179(11):7358–7364.
36. Swainson L, Kinet S, Manel N, Battini JL, Sitbon M, Taylor N. Glucose transporter 1 expression identifies a population of cycling CD4+ CD8+ human thymocytes with high CXCR4-induced chemotaxis. *Proc Natl Acad Sci U S A*. 2005;102(36):12867–12872.
37. Poznansky MC, et al. Thymocyte emigration is mediated by active movement away from stroma-derived factors. *J Clin Invest*. 2002;109(8):1101–1110.
38. Vianello F, Kraft P, Mok YT, Hart WK, White N, Poznansky MC. A CXCR4-dependent chemorepellent signal contributes to the emigration of mature single-positive CD4 cells from the fetal thymus. *J Immunol*. 2005;175(8):5115–5125.
39. Annunziato F, et al. Macrophage-derived chemokine and EBI1-ligand chemokine attract human thymocytes in different stage of development and are produced by distinct subsets of medullary epithelial cells: possible implications for negative selection. *J Immunol*. 2000;165(1):238–246.
40. Nakano H, Mori S, Yonekawa H, Nariuchi H, Matsuzawa A, Kakiuchi T. A novel mutant gene involved in T-lymphocyte-specific homing into peripheral lymphoid organs on mouse chromosome 4. *Blood*. 1998;91(8):2886–2895.
41. Benz C, Heinzel K, Bleul CC. Homing of immature thymocytes to the subcapsular microenvironment within the thymus is not an absolute requirement for T cell development. *Eur J Immunol*. 2004; 34(12):3652–3663.
42. Uehara S, Grinberg A, Farber JM, Love PE. A role for CCR9 in T lymphocyte development and migration. *J Immunol*. 2002;168(6):2811–2819.
43. Wurbel MA, et al. Mice lacking the CCR9 CC-chemokine receptor show a mild impairment of early T- and B-cell development and a reduction in T-cell receptor gammadelta(+) gut intraepithelial lymphocytes. *Blood*. 2001;98(9):2626–2632.
44. Salomon DR, et al. Constitutive activation of integrin alpha 4 beta 1 defines a unique stage of human thymocyte development. *J Exp Med*. 1994; 179(5):1573–1584.
45. Mojcik CF, Salomon DR, Chang AC, Shevach EM. Differential expression of integrins on human thymocyte subpopulations. *Blood*. 1995; 86(11):4206–4217.
46. Bousso P, Robey E. Dynamics of CD8+ T cell priming by dendritic cells in intact lymph nodes. *Nat Immunol*. 2003;4(6):579–585.
47. Mempel TR, Henrickson SE, Von Andrian UH. T-cell priming by dendritic cells in lymph nodes occurs in three distinct phases. *Nature*. 2004; 427(6970):154–159.
48. Stoll S, Delon J, Brotz TM, Germain RN. Dynamic imaging of T cell-dendritic cell interactions in lymph nodes. *Science*. 2002;296(5574):1873–1876.
49. Killeen N, Sawada S, Littman DR. Regulated expression of human CD4 rescues helper T cell development in mice lacking expression of endogenous CD4. *EMBO J*. 1993;12(4):1547–1553.
50. LaFace DM, et al. Human CD8 transgene regulation of HLA recognition by murine T cells. *J Exp Med*. 1995;182(5):1315–1325.
51. Salter RD, et al. A binding site for the T-cell co-receptor CD8 on the alpha 3 domain of HLA-A2. *Nature*. 1990;345(6270):41–46.
52. Lee YJ, et al. Generation of PLZF+ CD4+ T cells via MHC class II-dependent thymocyte-thymocyte interaction is a physiological process in humans. *J Exp Med*. 2010;207(1):237–246.
53. Onuffer JJ, Horuk R. Chemokines, chemokine receptors and small-molecule antagonists: recent developments. *Trends Pharmacol Sci*. 2002;23(10):459–467.
54. Grusby MJ, et al. Mice lacking major histocompatibility complex class I and class II molecules. *Proc Natl Acad Sci U S A*. 1993;90(9):3913–3917.
55. Dzhagalov IL, Melichar HJ, Ross JO, Herzmark P, Robey EA. Two-photon imaging of the immune system. *Curr Protoc Cytom*. 2012;Chapter 12:Unit12.26.